

Speckle Interferometry at SOAR in 2023

ANDREI TOKOVININ,¹ BRIAN D. MASON,² RENE A. MENDEZ,³ AND EDGARDO COSTA³

¹*Cerro Tololo Inter-American Observatory — NFSs NOIRLab Casilla 603, La Serena, Chile*

²*U.S. Naval Observatory, 3450 Massachusetts Ave., Washington, DC, USA*

³*Universidad de Chile, Casilla 36-D, Santiago, Chile*

ABSTRACT

Results of the speckle-interferometry observations at the 4.1 m Southern Astrophysical Research Telescope (SOAR) obtained during 2023 are presented: 1913 measurements of 1533 resolved pairs or subsystems (median separation $0''.16$) and non-resolutions of 552 targets; 42 pairs are resolved here for the first time. This work continues our long-term effort to monitor orbital motion in close binaries and hierarchical systems. A large number (147) of orbits have been determined for the first time or updated using these measurements. Complementarity of this program with the Gaia mission is highlighted.

Keywords: binaries:visual

1. INTRODUCTION

This paper continues the series of double-star measurements made at the 4.1 m SOuthern Astrophysical Research Telescope (SOAR) since 2008 with the speckle camera, HRCam. Previous results are published by Tokovinin et al. (2010b, hereafter TMH10) and in (Tokovinin et al. 2010a; Hartkopf et al. 2012; Tokovinin 2012; Tokovinin et al. 2014, 2015a, 2016, 2018, 2019, 2020, 2021, 2022; Mason et al. 2023). Observations reported here were made during 2023.

The Gaia space mission (Gaia Collaboration et al. 2016) is having a profound impact in many areas, including binary stars, so it is appropriate to place our ongoing program in this context. Figure 1 plots separations and magnitude differences of pairs measured at SOAR in 2023. The green shading indicates pairs expected to be resolved by the 1 m Gaia apertures at the diffraction limit of $0''.1$; their individual measurements will become available in future data releases, while for wider pairs to the right of the shaded zone the positions of both components are already available in the current Gaia data release 3 (GDR3, Gaia Collaboration et al.

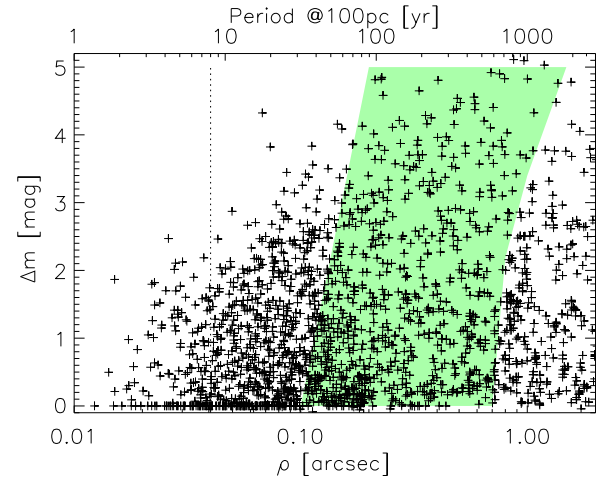


Figure 1. Magnitude difference Δm vs. separation ρ for pairs measured in 2023 (crosses). The upper axis indicates periods of binaries with such separations and a mass sum of $1 M_{\odot}$ if located at 100 pc distance. The hatched area highlights expected future measurements from Gaia, the vertical dotted line shows the SOAR diffraction limit in the I band.

2021). At a distance of 100 pc, $0''.1$ separation corresponds to orbital periods on the order of 30 yr which are common for low-mass binaries. Ground-based speckle interferometry is the only source of data for tracing orbits of such pairs, and our program makes a significant contribution here. The expected duration of the full

andrei.tokovinin@noirlab.edu

brian.d.mason.civ@us.navy.mil

rmendez@uchile.cl

Gaia mission will not suffice for derivation of astrometric or spectroscopic orbits with periods longer than ~ 10 yr, but the combination of the Gaia and ground-based data opens exciting perspectives for accurate measurements of stellar masses and for other applications.

The structure and content of this paper are similar to other papers of this project. Section 2 reviews all speckle programs that contributed to this paper, the observing procedure, and the data reduction. The results are presented in Section 3 in the form of electronic tables archived by the journal. We also discuss new resolutions and present orbits resulting from this data set. A short summary and an outlook of further work in Section 4 close the paper.

2. OBSERVATIONS

2.1. Observing Programs

As in previous years, HRCam (see Section 2.2) was used during 2023 to execute several observing programs, some with common targets. In the data tables, new or recently discovered objects are linked to respective programs by labels in place of usual discoverer designations (that are not yet assigned), see Section 3.1. They are also marked by tags, where N means new pair resolved in 2023, and other tags refer to pairs resolved previously but not yet published.

Hierarchical systems are currently the core of our program. Their architecture is relevant to star formation, while dynamical evolution of these hierarchies increases chances of stellar interactions and mergers (Tokovinin 2021a). Orbital motions of many triple systems are monitored at SOAR, and these data are used for orbit determinations and dynamical analysis (Tokovinin & Latham 2020; Tokovinin 2021b, 2023a,b). We re-observed some tight inner subsystems of hierarchies discovered at SOAR in 2021-2022 by Powell et al. (2023, label POW, tag P) and hierarchies within 100 pc Tokovinin (2023c, label GKM, tag T), see Section 3.5. Wider pairs within 100 pc resolved by Gaia but not yet featured in the WDS were observed in search for inner subsystems (tag G). Also, on request by S. Majewski, we targeted several doubly eclipsing quadruples discovered from the TESS photometry by Kostov et al. (2022); these stars are labeled QUAD in the data tables. New data on all hierarchical systems are reflected in the Multiple Star Catalog, MSC (Tokovinin 2018a). Its latest update in 2023 December is available at the MSC [home page](#) and at [Vizier](#).

Orbits of resolved binaries are improved in quantity and quality using our new measurements, contributing to the [Sixth Catalog of Orbits of Visual Binary Stars](#) (Hartkopf et al. 2001). We provide large tables of re-

liable and preliminary orbits in Section 3.3. Data on visual orbits serve in many areas, e.g. to probe alignment of exoplanetary orbits (Lester et al. 2023).

Hipparcos binaries within 200 pc are monitored to measure masses of stars and to test stellar evolutionary models, as outlined by, e.g., Horch et al. (2015, 2017, 2019). The southern part of this sample is addressed at SOAR (Mendez et al. 2017). This program overlaps with the general work on visual orbits.

Nearby M dwarfs are being observed at SOAR since 2018 following the initiative of T. Henry and E. Vrijmoet. The goal is to assemble statistical data on orbital elements, focusing on short periods. First results on M dwarfs are published by Vrijmoet et al. (2022). In 2023, we continued to monitor these pairs; a paper containing ~ 50 orbits of M dwarfs is in preparation. In anticipation, residuals to some of those orbits are given in the data table. Measurements of previously known pairs are published here, and those of new pairs from Vrijmoet et al. (2022) are deferred to the paper on orbits. In 2023, a modest number of additional low-mass M dwarfs within 25 pc were targeted (labeled as M25), and two were resolved.

Neglected close binaries from the Washington Double Star Catalog, WDS (Mason et al. 2001),¹ were observed as a “filler” at low priority.

TESS follow-up continues the program executed in 2018–2020, at a reduced rate. Its past results are published by Ziegler et al. (2020, 2021). All speckle observations of TESS targets of interest are promptly posted on the [EXOFOF web site](#). These data are used in the growing number of papers on TESS exoplanets, mostly as limits on close companions to exohosts. We publish here measures of four pairs from the TESS program resolved for the first time in 2023 and lacking relative positions in GDR3 (tag Z).

Acceleration stars were observed in 2021-2022 as potential targets of high-contrast imaging of exoplanets in a program led by K. Franson and B. Bowler (tag A). While their paper is still in preparation, we re-observed many of resolved targets in 2023 to confirm the detections and to clarify their nature.

A few close subsystems in *wide pairs* resolved previously in the program led by J. Chanamé (tag C) have been re-observed in 2023 to detect orbital motion, while their first resolutions still await publication.

Speckle observations in 2023 were conducted during 9 observing runs for a total of approximately 9 nights (7.5 allocated nights and 1.5 nights of engineering time).

¹ See the latest [online](#) WDS version.

Two additional nights allocated by the SOAR partners for the TESS follow-up were lost to clouds. The seeing in the second half of 2023 has been consistently worse than usual, often precluding observations of faint targets.

2.2. Instrument, Observing Procedure, and Data Processing

The observations reported here were obtained with the *high-resolution camera* (HRCam) — a fast imager designed to work at the 4.1 m SOAR telescope (Tokovinin 2018b). The instrument and observing procedure are described in the previous papers of these series (e.g. Tokovinin et al. 2020) and briefly summarized by Mason et al. (2023). There is no need to repeat the same text here. We used mostly the near-infrared *I* filter (824/170 nm), while the Strömgren *y* filter (543/22 nm) was used for brighter and/or closer pairs. Calibration of the pixel scale and orientation is based on a set of wide binaries with well-modeled motion, linked to the Gaia astrometry. Typical external errors of positional measurements, evaluated from the calibrators and from residuals to orbits, are 1-2 mas; the errors are larger for pairs with large contrast or faint magnitudes. The total number of HRCam observations made since 2008 approaches 40 000 (26 331 measurements and 12 965 non-resolutions).

The diffraction limit λ/D of the 4.1 m SOAR telescope in the *y* and *I* filters is 27 and 41 mas, respectively. However, as shown in Figure 1, many pairs at closer separations were measured. Their positions are obtained by modeling the speckle power spectra of the target and of the reference star. Below the diffraction limit, only part of the elongated central fringe is accessible, and the resulting positions become less accurate (they are marked by colons). Nevertheless, the closest pairs are also the fastest, and even less accurate data are useful for tracing their orbital motion.

3. RESULTS

3.1. Data Tables

The results (measures of resolved pairs and non-resolutions) are presented in almost the same format as in Mason et al. (2023). The long tables are published electronically; here we describe their content.

A note on system designations is needed here. The historic data on double stars in the WDS database (Mason et al. 2001) use a tradition of assigning each pair a unique Discoverer Designation (DD), linking it to the first published measurement. For example, COU 929 indicates that this pair has been discovered visually by

Table 1. Measurements of Double Stars at SOAR

Col.	Label	Format	Description, units
1	WDS	A10	WDS code (J2000)
2	Discov.	A16	Discoverer Designation
3	Other	A16	Alternative name
4	RA	F8.4	R.A. J2000 (deg)
5	Dec	F8.4	Declination J2000 (deg)
6	Epoch	F9.4	Julian year (yr)
7	Filt.	A2	Filter
8	N	I2	Number of averaged cubes
9	θ	F8.1	Position angle (deg)
10	$\rho\sigma_\theta$	F5.1	Tangential error (mas)
11	ρ	F8.4	Separation (arcsec)
12	σ_ρ	F5.1	Radial error (mas)
13	Δm	F7.1	Magnitude difference (mag)
14	Flag	A1	Flag of magnitude difference ^a
15	Tag	A1	System tag ^b
16	$(O-C)_\theta$	F8.1	Residual in angle (deg)
17	$(O-C)_\rho$	F8.3	Residual in separation (arcsec)
18	Ref	A9	Orbit reference ^c

^a Magnitude Flags: q – the quadrant is determined; * – Δm and quadrant from average image; : – noisy data or tentative measures.

^b System tags: A – Hipparcos-Gaia acceleration stars (K. Franson); C – Wide pairs observed for J. Chanamé; G – Wide pairs with relative positions in Gaia DR3; N – New pair resolved in 2023; P – Hierarchical systems from Powell et al. (2023); T – Hierarchies within 100 pc (Tokovinin 2023c); Z – TESS objects of interest (Ziegler et al. 2021).

^c Orbit References are provided at https://crf.usno.navy.mil/data_products/WDS/orb6/wdsref.html

Table 2. Unresolved Stars

Col.	Label	Format	Description, units
1	WDS	A10	WDS code (J2000)
2	Discov.	A16	Discoverer Designation
3	Other	A16	Alternative name
4	RA	F8.4	R.A. J2000 (deg)
5	Dec	F8.4	Declination J2000 (deg)
6	Epoch	F9.4	Julian year (yr)
7	Filt.	A2	Filter
8	N	I2	Number of averaged cubes
9	ρ_{\min}	F7.3	Angular resolution (arcsec)
10	$\Delta m(0.15)$	F7.2	Max. Δm at $0''.15$ (mag)
11	$\Delta m(1)$	F7.2	Max. Δm at $1''$ (mag)

P. Couteau. In the modern epoch, most new pairs are identified in surveys such as Hipparcos or Gaia; WDS currently assigns them disparate DDs based on the first author of (usually multi-author) publications listing the pairs. Furthermore, new subsystems in multiple stars are often given “recycled” DDs of the wide pairs to which they belong, with modified components qualifiers.

Nowadays the DDs became obsolete and they are no longer used by the wider community. They have lost links both to the primary data source (e.g. Gaia) and to the original papers. In the WDS supplement, WDSS, the DDs are no longer assigned. The combination of the WDS code and component designations like A,B or Aa,Ab uniquely identifies each pair, and the DDs are redundant. Objects without existing DDs are identified in the data tables by the WDS codes, labels related to the observing programs (e.g. GKM, QUAD, or M25), and component designations if resolved.

Table 1 lists 1913 measures of 1533 resolved pairs and subsystems, including new discoveries. The pairs are identified by their WDS-style codes based on the J2000 coordinates and DDs adopted in the WDS catalog (Mason et al. 2001) or their substitutes, as well as by alternative names in column (3), mostly from the Hipparcos catalog. Equatorial coordinates for the epoch J2000 in degrees are given in columns (4) and (5) to facilitate matching with other catalogs and databases. Circumstances of this particular observation (Julian Year, filter, number of cubes), be it Table 1 or 2, are given in columns (6) through (8). In the case of resolved multiple systems, the positional measurements and their errors (columns 9–12) and magnitude differences (column 13) refer to the individual pairings between components, not to their photocenters. As in the previous papers of this series, we list the internal errors derived from the power spectrum modeling and from the difference between the measures obtained from two data cubes. The real (external) errors are usually larger, especially for difficult pairs with substantial Δm and/or with small separations.

The flags in column (14) indicate the cases where the true quadrant is determined (otherwise the position angle is measured modulo 180°), when the relative photometry of wide pairs is derived from the long-exposure images (this reduces the bias caused by speckle anisoplanatism), and when the data are noisy or the resolutions are tentative (see TMH10).

To facilitate identification of pairs that either have been resolved previously but remain unpublished or are published but not yet entered in the WDS, we provide in column (15) one-character tags as follows: A — acceleration stars (Franson, Bowler), C — wide pairs (Chanamé), G — wide pairs with relative positions in GDR3, N — new pairs resolved here for the first time (Section 3.2), P — hierarchical systems published by Powell et al. (2023), T — components of triple or higher-order hierarchies within 100 pc (Tokovinin 2023c), Z — TESS objects of interest (Ziegler et al. 2021). For those pairs, the column (2) contains program-related labels

and component’s pairings, e.g. GKM Aa,Ab, instead of DDs.

For binary stars with known orbits, the residuals to the latest orbit and its reference are provided in columns (16)–(18). Residuals close to 180° mean that the orbit swaps the brighter (A) and fainter (B) stars. However, in some binaries or triples the secondary is fainter in one filter and brighter in the other. In these cases, it is better to keep the historical identification of the components in agreement with the orbit and to provide a negative magnitude difference Δm .

The non-resolutions of 552 targets (mostly reference stars) are reported in Table 2. Its first columns (1) to (8) have the same meaning and format as in Table 1. Column (9) gives the minimum resolvable separation when pairs with $\Delta m < 1$ mag are detectable. It is computed from the maximum spatial frequency of the useful signal in the power spectrum and is normally close to the formal diffraction limit λ/D . The following columns (10) and (11) provide the indicative dynamic range, i.e., the maximum magnitude difference at separations of $0''.15$ and $1''$, respectively, at 5σ detection level.

3.2. New Pairs

Newly resolved pairs are marked by the tag N in Table 1, so there is no need to give their separate list. There are 61 measures with this tag referring to 38 pairs (some of them have multiple measures). This does not include the wider pairs with tag G present in the GDR3 but not yet recognized as such in the WDS. Comments on 11 new subsystems in nearby hierarchies (label GKM) are given below in Section 3.5. Four new pairs from the TESS program have tags Z, so the total number of first-time resolutions is 42.

Two subsystems in nearby triple M-type dwarfs, 18113–7859 and 20253–2259, have been discovered in 2019.5 and 2022.4, respectively. Their measures should have been published by Vrijmoet et al. (2022), but were omitted owing to a technical oversight, while the outer pairs were reported. All measures of these subsystems are published here. The first pair has an orbit with a period of 1.7 yr that will appear in the forthcoming paper by Vrijmoet et al.

Of the 22 observed doubly eclipsing quadruples (label QUAD) from the paper by Kostov et al. (2022), 10 were resolved. These stars are mostly faint, early-type, and distant. The resolved objects are entered in the MSC as 2+2 quadruples, but in fact they may be higher-order hierarchies if the resolved secondaries are not eclipsing, while the doubly eclipsing objects belong to the brighter primaries.

As noted above, we observed 15 candidate faint M dwarf binaries within 25 pc (label M25). Two were resolved. The resolution of 01465–5340 at 0′′03 is tentative (it has been confirmed in 2024), while 03287–1537 is resolved securely at 0′′33.

As in the previous years, we discovered that a few Hipparcos stars observed as point-source references had close and faint companions (HIP 8387, 9534, 41375, 47070, 72640). One of those, HIP 47070, also has a physical companion BD–18° 2729 at 51′′4. The estimated period of the inner 0′′23 pair Aa,Ab is 60 yr, and its GDR3 astrometry does not show (yet) deviations from the linear motion. Other resolved Hipparcos stars were targeted on purpose because they had strong indications of binarity in the Gaia data (HIP 16526, 37505, 42728, 96562).

01350–0430 Aa,Ab is the brighter ($V = 14.98$ mag) component of the 40′′ nearby pair LDS 5338 AB at 80 pc from the Sun. It was observed on suggestion by D. Nazor who noted that GDR3 contains two equal stars at 0′′35 separation. Star A was indeed resolved at 0′′307. This triple is added to the MSC. The distant companion LDS 5338 B is a white dwarf.

The star BD–17° 1383 (06100–1702) has been observed as potential target for long-baseline interferometry; its resolution at 0′′028 is below the estimated detection limit and might be spurious. Another interferometric candidate 18042–6430 was resolved at 0′′037 in 2023.325, but found single in 2023.663; its estimated period is 1 yr.

12592–6256 Aa,Ab (HIP 63377) has been resolved by the speckle camera at the Gemini-S telescope (R. Mendez, 2023, private communication) and is confirmed here, while the wider companion at 0′′45 (TOK 422) has been discovered at SOAR in 2016. The estimated period of the inner pair is 3 yr, double lines were noted in its spectrum, although GDR3 does not give yet its orbit. This is another solar-type triple within 100 pc.

21199–5327 Ba,Bb is the secondary star in the bright binary θ Indi (HJ 5258 AB, 7′′3). H. Zirm (2023, private communication) has computed astrometric orbit of the subsystem Ba,Bb with a period of 26 yr and suggested that it should be resolvable by speckle interferometry. His prediction has been confirmed in 2023.32 and 2023.57. The magnitude difference of Ba,Bb is 5.4 mag in y and 3.7 mag in I , and the masses of Ba and Bb estimated from their absolute magnitudes are 1.08 and 0.54 M_{\odot} , respectively. According to the Zirm’s orbit, Ba,Bb is closing down and it will pass through the periastron in 2027.3. The brighter star A has been reportedly resolved in 2012.56 at 62 mas and designated as

MRN 3Aa,Ab (Marion et al. 2014). However, this resolution, never confirmed, is likely spurious, considering the constant radial velocity of star A (Lagrange et al. 2009) and its good Gaia astrometry.

3.3. New and Updated Orbits

The seven Campbell orbital elements were fitted to all available positional measurements using the IDL code `orbit` (Tokovinin 2016). The weights are inversely proportional to the squares of the position errors, assumed to be 2 mas for the SOAR data (larger for fainter stars or pairs with large contrast), 5 mas for other speckle data, and 0′′05 or larger for visual measurements. The $\chi^2/(N - M)$ goodness-of-fit parameter is typically on the order of one, indicating that the adopted errors are approximately correct. When the orbit is poorly constrained, some elements are fixed to values that match both the positions and the expected mass sum, computed with parallaxes from GDR3 or other sources. The longitude of periastron ω is fixed to zero in the degenerate cases of circular or face-on orbits. Note that in our previous paper (Mason et al. 2023), the orbits were calculated using a different tool and a different weighting scheme.

The list of 147 computed orbits is divided into two groups, reliable (87) and preliminary (60), using criteria outlined by Mason et al. (2023). In these Tables 3 and 4, the system is identified by the WDS J2000 coordinate and the DD (when available), followed by the seven Campbell elements. The two rightmost columns contain the orbit grade and a reference to the most current orbit which has been here improved, when available; the first-time orbits are referenced as SOAR2023. The grades are assigned by the standard method described by Hartkopf et al. (2001), which includes both the rms residual as well as the phase or position angle coverage, total number of measures, and the total number of orbits. The grades do not always correlate with the quality metrics based strictly on absolute or relative errors of the elements determined by the least-squares fits, so that some orbits in Table 3 would be considered preliminary by their grades of 4 and 5. In Table 3 the errors of each orbital element are listed in the subsequent line below the main entry, while in Table 4 the errors are not provided.

Many orbits in the present lists are based exclusively on the positions measured at SOAR. It would be desirable to obtain data on these pairs from other teams for a cross-check. Some pairs (04237+1131 and others) are Hipparcos “problem” stars (suspected non-single, acceleration, or stochastic solutions).

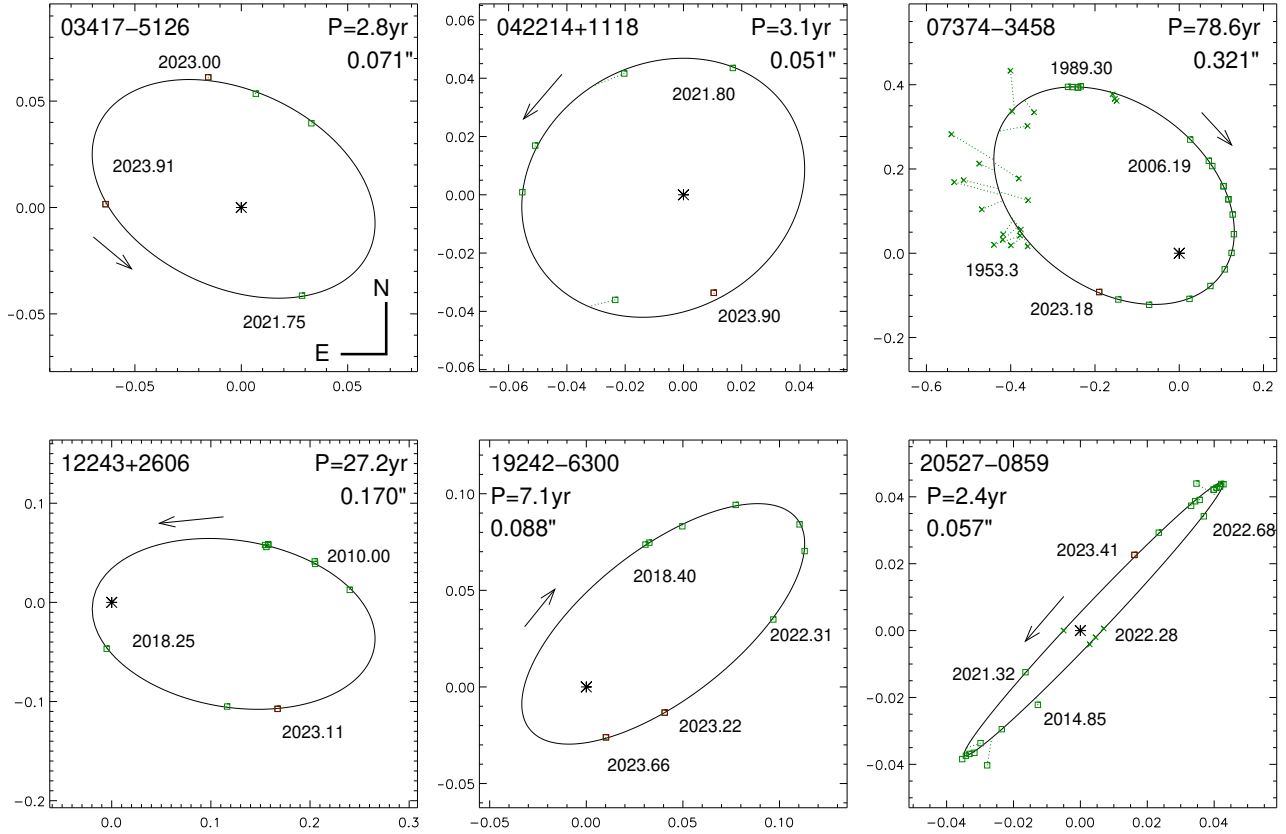


Figure 2. Six new visual orbits with well-constrained orbital elements. In each plot, the ellipse shows the fitted orbit, squares connected to the ellipse are accurate speckle data, while visual measures and non-resolutions are shown as crosses. The primary component (asterisk) is at coordinate origin, the axis scale is in arcseconds. Orientation, periods, semimajor axes, and sense of rotation are indicated.

Figure 2 contains illustrative plots of six visual orbits computed here for the first time (except one), but nevertheless well constrained. The pair 03417–5126 is a Hipparcos star with acceleration, first resolved at SOAR in 2021 (tag A, to be published by Franson and Bowler); its preliminary orbit is based on five measures covering more than half of the 2.8 yr period. Regular monitoring of 04224+1118, a neglected binary in the Hyades (PAT 5), enables calculation of the first orbit. The orbit of 07374–3458 (FIN 324AC) is an update of the previous solution (Tokovinin et al. 2015a). It highlights the vastly improved accuracy of the speckle data compared to the historic visual measurements. The SOAR data from 2008 to 2023 cover the periastron, and no substantial orbit improvement is expected in the coming decade. Note that the pair FIN 324AB listed in the WDS is spurious. If it were real, it would make the triple system unstable and would certainly affect the observed motion of AC, which shows no deviations from the orbit apart from the measurement errors (the weighted residuals are 2 mas). The pair 12243+2606 has been resolved by the Yale speckle program (YSC 97), but most data come

from SOAR; the measures of 19242–6300 (TOK 799) come only from this program. Finally, the orbit of the bright speckle binary 20527–0859 (McA 64 Aa,Ab) has not been determined previously despite many measures because of the short period (2.4 yr) and the lack of frequent visits. The puzzle has been eventually solved with the help of the dense coverage at SOAR, including the times of non-resolutions; four positions corresponding to non-resolutions are plotted by crosses in Figure 2 only for illustration. The quality of this orbit is excellent, with weighted residuals of 1 mas (some old speckle data were given reduced weights). Yet, the official grade is only 4, illustrating a limitation of the current grading system and possibly an over-reliance on the total number of measures and the total phase coverage. The 4.3 yr spectroscopic orbit of this star by Abt & Levy (1985) is spurious; a plot of their RVs phased with the correct period reveals only noise.

Below we comment on some other pairs with new orbits.

05321–0305 (V1311 Ori) is a system of pre-main sequence M-type dwarfs containing at least six stars

(Tokovinin 2022). The updated 150 yr orbit of Aa,Ab uses measures near the periastron recently published by Calissendorff et al. (2022) and the latest SOAR data, but it will remain loosely constrained until the binary approaches the apastron in a few decades. On the other hand, the tentative 8 yr orbit of the faster pair Ba,Bb discovered at SOAR in 2021 will become well-defined in the next few years.

09525–0806 (HR 3909). The very bright double star γ Sex was first split by Alvan Clark in 1854 while testing his telescopes (Clark & Dawes 1857). The first resolution of this pair and others, and the praise given to his telescopes by W. R. Dawes led to Clark and his sons getting many orders for telescopes and constructing the largest telescope in the world six different times in the 19th and early 20th centuries. The first accurate measure would wait more than two decades until Hall (1892) used a larger Clark refractor. We update the previous 77.8 yr orbit by Brendley & Mason (2007) using accurate speckle measures; its further improvement

is foreseen as the pair goes through the periastron in 2034.

13175+2024 (YSC 149) is a resolved triple system where the inner pair Aa,Ab has a period around 5 yr. Pending the full analysis, a preliminary 33 yr outer orbit is given here in Table 4.

16090–0939 (HIP 79122) is a γ Dor variable of spectral type A8V, originally observed at the request of Frank Fekel. The composite spectrum revealed evidence of two stars (Henry et al. 2011). This binary was first measured in 2008 with an early version of HRCam, when the USNO speckle camera did not arrive at CTIO in time for observing on the Blanco telescope. The pair with $\Delta m \sim 3.5$ mag is not resolved at close separations near the periastron, the eccentricity is large but not well constrained, so it was fixed at $e = 0.97$ to obtain the mass sum around $5 \mathcal{M}_{\odot}$ with the GDR3 parallax of 12.57 ± 0.09 mas.

Table 3. Visual Orbits with well-defined Errors

WDS	Discoverer	P	T	e	a	Ω	ω	i	Grade	Ref.
α, δ (2000)	Designation	(yr)	(yr)		(arcsec)	(deg)	(deg)	(deg)		
00026+1841	HDS 2 Aa,Ab	22.68 ± 0.34	2020.967 ± 0.074	0.631 ± 0.013	0.1106 ± 0.0028	17.4 ± 2.3	302.2 ± 3.1	59.8 ± 1.3	3	SOAR2023
00061+0943	HDS 7	51.23 ± 1.11	2003.83 ± 0.11	0.534 ± 0.014	0.2145 ± 0.0032	184.1 ± 1.1	237.1 ± 2.1	60.0 ± 0.9	3	FRM2017c
00098–3347	SEE 3	295.7 ± 8.6	1978.66 ± 0.48	0.770 ± 0.009	0.928 ± 0.020	274.3 ± 3.4	72.5 ± 3.4	33.1 ± 2.0	4	Hrt2010a
00111+0513	TOK 869	8.49 ± 0.10	2018.22 ± 0.18	0.183 ± 0.018	0.1112 ± 0.0029	108.8 ± 2.0	239.7 ± 8.0	51.2 ± 1.8	4	Tok2023a
00135–3650	HDS 32	15.272 ± 0.054	2009.080 ± 0.078	0.242 ± 0.005	0.2233 ± 0.0016	101.2 ± 3.8	266.0 ± 3.4	159.6 ± 1.8	2	Tok2017b
00143–2732	HDS 33	10.150 ± 0.016	2013.465 ± 0.017	0.608 ± 0.004	0.1222 ± 0.0010	33.3 ± 2.7	82.5 ± 2.4	27.6 ± 1.1	2	Tok2015c
01017+2518	HDS 134	16.563 ± 0.056	2015.209 ± 0.070	0.396 ± 0.012	0.1303 ± 0.0017	237.1 ± 0.7	288.0 ± 0.6	59.0 ± 0.7	2	A1W2014
01150–0908	UC 527 Aa,Ab	3.09 ± 0.21	2022.40 ± 0.09	0.40 ± 0.05	0.0407 ± 0.0029	110.5 ± 9.5	260.2 ± 7.0	51.5 ± 6.0	4	SOAR2023
01158–6853	I 27 CD	85.14 ± 0.21	2001.25 ± 0.92	0.040 ± 0.002	1.0877 ± 0.0054	140.6 ± 0.9	132.6 ± 3.3	31.1 ± 0.3	3	Izm2019
01406+0846	TOK 872	5.979 ± 0.026	2004.600 ± 0.004	0.710 ± 0.006	0.0770 ± 0.0025	122.9 ± 2.6	245.6 ± 0.8	60.3 ± 2.0	3	SOAR2023
01497–1022	BU 1168	121.0 ± 3.5	1924.56 ± 3.48	0.700 fixed	0.2949 ± 0.0119	205.5 ± 0.7	106.8 ± 2.5	94.9 ± 0.6	4	SOAR2023
02166–5026	TOK 185	10.572 ± 0.062	2012.51 ± 0.80	0.023 ± 0.007	0.0907 ± 0.0025	266.6 ± 2.2	338.9 ± 27.3	47.1 ± 1.4	2	Tok2022f
02167+0632	YSC 20	13.291 ± 0.045	2010.630 ± 0.053	0.418 ± 0.008	0.1254 ± 0.0021	45.9 ± 6.6	31.2 ± 7.0	27.4 ± 3.8	3	Hor2021
02405–2408	SEE 19	307.2	2016.76	0.832	0.379	235.5	81.6	148.0	3	Tok2015c

Table 3 continued

Table 3 (continued)

WDS	Discoverer	P	T	e	a	Ω	ω	i	Grade	Ref.
α, δ (2000)	Designation	(yr)	(yr)		(arcsec)	(deg)	(deg)	(deg)		
		± 24.4	± 0.05	± 0.009	± 0.020	± 2.7	± 3.1	± 1.4		
02415–1506	HDS 351	42.7	1979.8	0.374	0.241	24.2	294.6	88.8	3	Tok2022f
		± 6.0	± 6.5	± 0.041	± 0.025	± 0.5	± 17.0	± 0.4		
03309–6200	TOK 190	3.627	2021.081	0.445	0.0637	30.4	242.5	79.2	2	Tok2018i
		± 0.011	± 0.027	± 0.023	± 0.0011	± 0.8	± 1.8	± 0.8		
04224+1118	PAT 5	3.049	2024.18	0.162	0.0508	121.4	124.6	32.9	2	SOAR2023
		± 0.014	± 0.101	± 0.032	± 0.0020	± 9.5	± 11.3	± 9.4		
04279+2427	TOK 877	10.9	2015.15	0.192	0.156	85.9	221.1	63.1	4	SOAR2023
		± 1.0	± 0.25	± 0.089	± 0.012	± 3.4	± 10.4	± 3.1		
04506+1505	CHR 20	5.738	2003.825	0.048	0.0890	129.7	270.5	113.2	2	Doc2018h
		± 0.006	± 0.085	± 0.010	± 0.0010	± 0.7	± 5.2	± 0.6		
05301–3228	B 1946	67.2	2023.24	0.776	0.1140	180.2	358.7	34.9	3	Tok2022f
		± 4.0	± 0.07	± 0.008	± 0.0014	± 5.5	± 7.5	± 4.2		
05427–6708	I 745	205.1	2017.70	0.786	0.542	244.9	205.7	75.4	4	Tok2019c
		± 35.1	± 0.18	± 0.024	± 0.061	± 0.8	± 1.5	± 0.7		
06460–6624	TOK 826 CD	11.70	2023.000	0.621	0.0970	36.1	319.5	149.1	4	SOAR2023
		± 1.86	± 0.048	± 0.044	± 0.0051	± 11.6	± 14.5	± 8.9		
06481–0948	A 1056	113.6	1995.91	0.712	0.405	70.4	257.8	78.5	3	Tok2015c
		± 3.7	± 0.65	± 0.047	± 0.022	± 1.5	± 1.5	fixed		
07374–3458	FIN 324 AC	78.58	2016.772	0.656	0.3208	71.8	205.7	153.3	2	Tok2015c
		± 0.73	± 0.021	± 0.002	± 0.0023	± 1.7	± 1.6	± 0.7		
08250–4246	CHR 226 Ba,Bb	63.2	2018.04	0.502	0.0655	82.1	259.5	114.7	3	Tok2023d
		± 7.7	± 0.35	± 0.035	± 0.0054	± 2.0	± 7.8	± 2.5		
08277–0425	A 550	21.062	2002.583	0.844	0.0939	34.5	47.8	150.5	2	Tok2023a
		± 0.051	± 0.069	± 0.009	± 0.0027	± 8.2	± 8.3	± 3.8		
08313–0601	BAG 49 Aa,Ab	16.43	2007.60	0.718	0.247	122.0	253.6	72.7	3	SOAR2023
		± 0.13	± 0.14	± 0.046	± 0.021	± 2.3	± 1.8	± 1.9		
08375–5336	GKM Aa,Ab	2.90	2023.13	0.496	0.0520	66.4	199.9	41.7	3	SOAR2023
		± 0.22	± 0.005	± 0.048	± 0.0025	± 7.3	± 10.9	± 8.7		
09525–0806	AC 5 AB	77.61	1956.84	0.741	0.380	198.5	306.2	143.2	2	USN2007a
		± 0.59	± 0.69	± 0.019	± 0.013	± 5.2	± 6.5	± 3.4		
10255–6504	HDS 1499	20.44	2022.053	0.782	0.0815	130.1	132.9	36.4	3	Tok2023a
		± 0.73	± 0.055	± 0.010	± 0.0019	± 4.7	± 5.4	± 3.8		
11238–3829	CHR 241	3.530	2013.182	0.380	0.0582	155.7	254.8	111.8	2	Tok2016e
		± 0.009	± 0.031	± 0.019	± 0.0009	± 1.0	± 1.4	± 0.9		
12018–3439	I 215 AB	178.48	2016.29	0.407	0.862	269.8	268.4	111.3	3	Tok2015a
		± 4.50	± 0.43	± 0.006	± 0.015	± 0.3	± 2.3	± 0.3		
12104–4352	TOK 897	12.76	2017.90	0.597	0.0630	86.1	101.8	50.2	3	Tok2022f
		± 0.69	± 0.05	± 0.023	± 0.0025	± 3.3	± 3.4	± 2.0		
12114–1647	S 634 Aa,Ab	0.5792	2018.7250	0.2809	0.0253	49.3	284.2	43.8	2	SOAR2023
		± 0.0006	± 0.0007	± 0.0018	± 0.0021	± 4.2	± 0.5	± 8.6		
12243+2606	YSC 97	27.25	2017.80	0.868	0.170	164.0	275.1	32.3	4	Tok2023d
		± 1.76	± 0.11	± 0.021	± 0.012	± 8.2	± 7.1	± 7.3		
12386–2704	BWL 32	17.85	2019.996	0.334	0.2296	188.5	74.3	135.2	3	Tok2022f
		± 0.65	± 0.093	± 0.016	± 0.0046	± 3.1	± 5.7	± 1.6		
12455–4552	HDS 1789 Aa,Ab	23.41	2024.00	0.248	0.127	33.8	357.7	33.2	3	Tok2023d
		± 0.45	± 0.38	± 0.059	± 0.005	± 13.5	± 21.4	± 5.4		
12479–5127	TOK 720	10.78	2023.77	0.292	0.0505	85.7	134.1	152.2	3	Tok2022f
		± 1.14	± 0.18	± 0.084	± 0.0045	± 16.1	± 15.1	± 11.1		
12528+1225	TOK 401	9.964	2015.56	0.097	0.1108	117.3	294.5	75.1	3	Tok2018b
		± 0.080	± 0.13	± 0.011	± 0.0010	± 0.6	± 5.0	± 0.6		
13132–0501	TOK 402	17.48	2016.694	0.583	0.1534	114.7	254.4	111.2	3	Tok2020g

Table 3 continued

Table 3 (continued)

WDS	Discoverer	P	T	e	a	Ω	ω	i	Grade	Ref.
α, δ (2000)	Designation	(yr)	(yr)		(arcsec)	(deg)	(deg)	(deg)		
		± 0.30	± 0.016	± 0.010	± 0.0014	± 0.4	± 0.7	± 0.5		
13133+1621	DOC 1	25.44	2014.81	0.424	0.0852	95.0	18.6	61.0	4	Doc2018h
		± 0.17	± 0.16	± 0.013	± 0.0018	± 2.1	± 4.2	± 3.6		
13513-2423	WSI 77	10.490	2009.258	0.342	0.2848	171.6	140.2	96.4	2	Tok2012b
		± 0.006	± 0.010	± 0.002	± 0.0006	± 0.1	± 0.4	± 0.1		
13598-0333	HDS 1962	9.776	2008.342	0.396	0.0791	37.0	233.1	56.7	2	Tok2019c
		± 0.056	± 0.057	± 0.011	± 0.0010	± 1.2	± 1.7	± 0.8		
14219-3126	BWL 38	9.77	2020.221	0.371	0.0997	236.8	287.0	106.0	3	Tok2022f
		± 0.15	± 0.093	± 0.035	± 0.0029	± 1.9	± 4.5	± 2.3		
14453-3609	I 528 AB	15.95	2023.47	0.628	0.0484	226.5	76.1	32.8	2	Tok2022a
		± 0.17	± 0.11	± 0.045	± 0.0038	± 12.2	± 10.5	± 9.2		
14509-1603	BEU 19 Ba,Bb	16.229	2021.95	0.244	0.346	122.7	184.1	54.4	4	Tok2023d
		± 0.043	± 0.12	± 0.008	± 0.006	± 1.4	± 3.3	± 1.5		
15006+0836	YSC 8 AB	6.922	2016.878	0.375	0.1163	149.4	99.7	95.9	2	Tok2018
		± 0.003	± 0.007	± 0.002	± 0.0006	± 0.3	± 0.4	± 0.3		
15071-0217	A 689	67.26	1994.46	0.671	0.2194	145.1	12.6	107.4	5	Doc2023
		± 0.92	± 0.41	± 0.015	± 0.0032	± 0.8	± 3.6	± 1.2		
15332-2429	SEE 238 Ba,Bb	61.70	1999.82	0.676	0.228	204.7	132.5	24.0	2	Msn2017a
		± 0.41	± 0.30	± 0.010	± 0.007	± 7.2	± 7.8	± 5.5		
15367-4208	TOK 408 Ca,Cb	7.97	2014.41	0.0	0.0570	102.0	0.0	62.9	4	Tok2018b
		± 0.16	± 0.15	fixed	± 0.0015	± 3.3	fixed	± 5.1		
15481-5811	SKF 2839 Aa,Ab	11.11	2023.771	0.565	0.1704	14.3	46.3	160.5	3	SOAR2023
		± 0.45	± 0.018	± 0.015	± 0.0020	± 10.6	± 8.4	± 6.8		
16054-1948	BU 947 AB	220.0	2054.5	0.685	0.851	80.2	242.2	75.7	3	Tok2017c
		fixed	± 3.5	± 0.021	± 0.032	± 1.5	± 1.8	± 0.9		
16054-1948	MCA 42 CE	18.953	2006.00	0.610	0.1047	108.0	80.8	45.4	2	Tok2018e
		± 0.064	± 0.12	± 0.010	± 0.0016	± 2.9	± 1.7	± 1.3		
16077-2125	MCA 43	11.32	2017.06	0.40	0.0476	143.0	199.9	81.6	5	SOAR2023
		± 0.11	± 0.68	± 0.11	± 0.0030	± 1.7	± 17.4	± 2.3		
16090-0939	WSI 85	9.51	2020.89	0.970	0.098	139.6	319.6	83.5	3	SOAR2023
		± 0.15	± 0.31	fixed	± 0.028	± 3.5	± 20.5	± 5.6		
16249-2240	KSA 129 Aa,Ab	13.13	2019.45	0.290	0.0584	67.5	143.0	165.2	3	Tok2023d
		± 0.34	± 0.37	± 0.048	± 0.0087	± 154.9	± 143.6	± 33.5		
16283-1613	RST3950	26.23	2000.66	0.808	0.157	88.7	210.7	157.9	3	Doc2009g
		± 0.17	± 0.35	± 0.018	± 0.006	± 16.1	± 16.6	± 12.8		
16458-0046	A 1141	31.15	2019.22	0.877	0.1140	302.1	106.9	164.0	2	Baz1976
		± 0.21	± 0.08	± 0.005	± 0.0034	± 21.5	± 20.5	± 8.8		
16488+1039	CRC 73	11.51	2021.16	0.176	0.200	27.6	187.5	71.4	3	Tok2022f
		± 0.38	± 0.26	± 0.019	± 0.006	± 1.6	± 8.4	± 0.9		
17415-5348	HDS 2502	20.32	2018.045	0.593	0.1341	158.8	322.0	136.4	2	Tok2019c
		± 0.22	± 0.027	± 0.006	± 0.0009	± 1.3	± 1.4	± 0.8		
18480-1009	HDS 2665	42.03	2023.906	0.313	0.4964	42.8	178.6	57.2	4	Tok2019c
		± 0.31	± 0.086	± 0.005	± 0.0019	± 0.5	± 1.8	± 0.4		
18520+1358	CHR 80	64.6	1990.18	0.662	0.161	98.5	280.2	121.4	3	Tok2023d
		± 3.1	± 0.84	± 0.052	± 0.020	± 2.4	± 2.3	± 5.4		
18520-5418	TOK 325 Aa,Ab	11.04	2017.45	0.241	0.1033	107.9	328.3	50.3	3	Tok2022f
		± 0.19	± 0.11	± 0.015	± 0.0020	± 2.1	± 4.1	± 1.7		
19035-6845	FIN 357	14.102	2018.104	0.383	0.1493	148.8	234.7	155.5	2	Doc2018i
		± 0.042	± 0.018	± 0.004	± 0.0010	± 3.5	± 3.8	± 1.4		
19040-3804	I 1391	48.75	2003.88	0.505	0.1868	123.4	194.7	52.3	3	Tok2015c
		± 0.72	± 0.59	± 0.028	± 0.0022	± 3.0	± 6.1	± 2.6		
19242-6300	TOK 799	7.12	2024.08	0.585	0.088	127.3	356.2	122.6	3	SOAR2023

Table 3 continued

Table 3 (continued)

WDS	Discoverer	P	T	e	a	Ω	ω	i	Grade	Ref.
α, δ (2000)	Designation	(yr)	(yr)		(arcsec)	(deg)	(deg)	(deg)		
		± 0.46	± 0.12	± 0.075	± 0.005	± 3.1	± 7.9	± 4.3		
19294-4057	B 1385	51.82	1978.32	0.100	0.1821	126.5	108.7	50.5	2	Tok2018b
		± 0.92	± 1.03	± 0.016	± 0.0015	± 1.5	± 4.1	± 0.9		
19377-4128	VOU 34	61.29	2001.24	0.065	0.1651	133.9	70.6	97.6	3	Tok2017c
		± 1.95	± 2.78	± 0.043	± 0.0032	± 0.4	± 17.1	± 0.6		
19453-6823	TOK 425 Ba,Bb	4.291	2017.128	0.85	0.0503	139.5	203.8	133.1	3	Tok2019c
		± 0.072	± 0.079	fixed	± 0.0046	± 12.9	± 20.7	± 9.7		
19563-3137	TOK 698	12.79	2015.93	0.164	0.1085	59.6	44.0	90.8	3	Tok2019c
		± 0.47	± 0.19	± 0.049	± 0.0040	± 0.4	fixed	± 0.5		
20216+1930	COU 327 AB	51.7	1987.21	0.46	0.1306	67.5	326.1	81.0	3	Doc2008a
		± 2.5	± 0.70	± 0.05	± 0.0037	± 0.9	± 11.6	± 1.5		
20217-3637	HDS 2908	12.699	2007.37	0.536	0.1113	107.9	336.2	81.8	2	Tok2016e
		± 0.056	± 0.11	± 0.007	± 0.0016	± 0.4	± 3.2	± 0.6		
20325-1637	SEE 512	42.62	2001.79	0.915	0.136	139.0	199.6	130.9	2	Doc2023
		± 0.72	± 0.95	± 0.032	± 0.011	± 19.0	± 27.8	± 6.5		
20527-0859	MCA 64 Aa,Ab	2.404	2018.973	0.150	0.0565	136.6	308.0	85.7	4	Tok2023d
		± 0.002	± 0.068	± 0.024	± 0.0008	± 0.7	± 9.8	± 1.2		
21130-1133	VOU 24 AB	161.4	2013.66	0.316	0.309	98.0	250.0	143.2	4	Tok2019c
		± 6.7	± 0.57	± 0.019	± 0.008	± 2.5	fixed	± 2.4		
21278-5922	TOK 731	12.99	2022.544	0.616	0.0600	198.0	128.6	27.6	3	Tok2022g
		± 0.62	± 0.036	± 0.015	± 0.0013	± 10.0	± 11.4	± 4.2		
21310-3633	B 1008 AB	75.05	2019.737	0.636	0.2222	32.3	163.3	102.9	4	Tok2018b
		± 1.91	± 0.113	± 0.007	± 0.0015	± 0.3	± 1.5	± 0.4		
21395-0003	BU 1212 AB	48.88	2020.814	0.861	0.4211	140.4	294.4	54.7	2	Tok2019c
		± 0.10	± 0.007	± 0.001	± 0.0018	± 0.3	± 0.3	± 0.3		
21477-3054	FIN 330 AB	20.23	2007.34	0.443	0.1232	32.5	216.5	108.8	2	Tok2019c
		± 0.13	± 0.08	± 0.012	± 0.0013	± 0.7	± 1.8	± 0.4		
21543+1943	COU 432 BC	62.9	2029.84	0.094	0.192	7.8	137.2	108.3	4	Tok2022f
		± 2.1	± 2.79	± 0.037	± 0.008	± 1.3	± 17.7	± 1.3		
22056-5858	B 548	36.92	2025.27	0.624	0.148	35.9	337.0	56.3	2	Tok2019c
		± 0.86	± 0.30	± 0.042	± 0.004	± 1.7	± 3.5	± 3.3		
22441+0644	TOK 703	4.887	2015.886	0.370	0.0588	170.5	343.3	135.4	3	Tok2019c
		± 0.064	± 0.090	± 0.039	± 0.0026	± 6.8	± 12.8	± 5.4		
22504-1744	DON 1038	163.0	1992.09	0.432	0.3934	137.7	0.0	0.0	4	Doc2016i
		± 5.6	± 0.61	± 0.017	± 0.0074	± 1.6	fixed	fixed		
23126+0241	A 2298 AB	29.161	2012.529	0.401	0.1989	287.0	312.9	102.7	2	Pbx2000b
		± 0.054	± 0.092	± 0.005	± 0.0013	± 0.3	± 1.1	± 0.3		
23179-0302	YSC 167	15.89	2016.52	0.63	0.077	35.2	137.8	98.3	4	Tok2023d
		± 0.61	± 1.80	± 0.16	± 0.028	± 4.7	± 41.4	± 4.6		
23285+0926	YSC 138	20.28	2008.12	0.539	0.0774	154.1	326.5	149.0	3	Tok2022f
		± 0.73	± 0.17	± 0.036	± 0.0022	± 13.5	± 18.5	± 7.3		
23350+0136	MEL 9 BC	35.23	2009.66	0.082	0.446	9.3	126.4	82.9	3	MaN2019
		± 0.94	± 1.18	± 0.012	± 0.012	± 0.4	± 13.2	± 0.2		

Table 4. Preliminary Visual Orbits

WDS	Discoverer	P	T	e	a	Ω	ω	i	Grade	Ref.
α, δ (2000)	Designation	(yr)	(yr)		(arcsec)	(deg)	(deg)	(deg)		
00036–3106	TOK 686	14.014	2013.792	0.233	0.1310	11.8	264.9	71.2	4	Tok2023d
00321–1218	HDS 71	62.190	2035.840	0.216	0.2734	124.9	320.2	131.5	4	Cve2017
01503–8714	HDS 247	100.000	2030.110	0.355	0.2056	90.8	92.5	115.4	4	SOAR2023
02035–0455	TOK 873	20.000	2019.042	0.111	0.2303	51.8	196.8	28.3	4	SOAR2023
02143–4952	TOK 815	9.196	2017.400	0.300	0.1446	273.4	111.7	78.0	4	SOAR2023
02297–0216	BU 519	1000.000	2033.675	0.800	1.0282	80.5	104.5	64.9	3	SOAR2023
02370–3056	RST 2283	143.078	1906.421	0.500	0.2762	33.8	54.0	53.8	4	SOAR2023
03417–5126	HIP 17255	2.791	2021.688	0.170	0.0709	65.7	124.8	49.1	4	Tok2023d
03571–0828	RST 4764	200.000	1995.313	0.243	0.2270	155.9	353.9	124.7	4	SOAR2023
04237+1131	LSC 30	72.551	2024.214	0.550	0.0861	52.2	58.8	50.0	4	Tok2023d
04249–3445	DAM 1313 Aa,Ab	32.310	2021.200	0.500	0.1520	108.4	352.4	55.0	5	SOAR2023
04493+2934	RAS 18	57.350	2026.540	0.174	0.1590	274.0	64.6	152.5	4	SOAR2023
04550+1436	HDS 634	48.287	2013.029	0.527	0.1007	61.4	103.5	160.0	3	SOAR2023
05286–4548	HDS 723	80.000	2016.917	0.937	0.1569	148.5	135.0	114.4	4	SOAR2023
05289–0318	DA 6	1800.000	1995.856	0.860	1.0924	68.8	167.6	46.9	4	Tok2015c
05321–0305	JNN 39 Aa,Ab	150.000	2019.445	0.859	0.7899	132.8	44.8	66.5	4	Tok2022x
05321–0305	JNN 39 Ba,Bb	7.795	2022.159	0.000	0.0801	75.9	0.0	31.8	4	SOAR2023
05418–5000	HU 1568	320.000	2019.186	0.327	1.0281	174.4	70.3	109.8	4	Hrt2011d
06236+1739	A 2517	300.000	1969.492	0.372	0.1866	26.7	139.0	105.5	4	Tok2017c
07558+1320	YSC 199	54.787	2008.175	0.000	0.1522	121.4	0.0	117.8	4	SOAR2023
08134–4534	TOK 832	9.666	2018.994	0.000	0.0410	183.7	0.0	108.5	3	SOAR2023
09033–7036	HEI 223 AB	21.882	2023.220	0.206	0.0861	88.4	301.2	109.2	3	Tok2022f
09095–5538	YMG 29	12.000	2025.409	0.124	0.0478	157.2	212.9	39.4	3	SOAR2023
09133–5529	ELP 24	33.172	2021.416	0.806	0.0949	124.8	163.3	150.5	4	SOAR2023
09180–5453	JNN 69 Aa,Ab	6.964	2020.846	0.381	0.0486	217.0	74.6	39.9	4	Tok2023d
09477+2036	COU 284	133.858	2068.313	0.880	0.4014	94.3	265.9	96.7	5	Doc2019c
09494+1832	HDS 1419	36.347	2021.487	0.962	0.1042	149.9	243.2	20.0	3	SOAR2023
09586–2420	TOK 437	15.000	2012.429	0.223	0.0652	112.6	90.2	92.3	3	SOAR2023
10227–2350	B 197	171.5	1986.73	0.684	0.216	134.3	212.6	20.0	4	SOAR2023
10356–4715	GKM Aa,Ab	1.499	2016.643	0.471	0.0223	83.5	137.5	103.4	5	SOAR2023
10406–5342	FIN 40	300.000	1927.108	0.200	0.3493	146.8	355.9	35.0	5	SOAR2023
10527+0029	TOK 893 BC	32.762	2001.454	0.199	0.2422	180.9	259.2	128.1	5	SOAR2023
11136–4749	HDS 1602	100.000	2042.495	0.400	0.3276	37.2	15.6	84.2	5	SOAR2023
11430–3933	RST 5358	151.850	2035.744	0.277	0.1466	168.2	125.0	160.0	4	SOAR2023
12175+0636	BU 796	172.137	1980.853	0.290	0.3257	94.4	353.0	84.5	3	SOAR2023
12349–0509	RST 4502	223.477	2006.343	0.200	0.2261	63.6	151.0	66.1	4	SOAR2023
12407–4803	TOK 849	10.622	2018.485	0.500	0.0899	236.1	180.0	15.3	4	SOAR2023
13175+2024	YSC 149 AB	32.959	2016.098	0.085	0.2151	118.3	311.2	143.4	4	SOAR2023
13229–7209	B 1736	73.039	1962.488	0.627	0.1628	156.4	324.4	54.2	4	Tok2023d
13377–2337	RST 2856 AB	200.000	2117.606	0.046	0.3502	103.6	15.6	79.9	3	Tok2016e
13401–6033	TOK 292 Ca,Cb	40.000	2019.059	0.267	0.1987	131.9	195.4	155.5	4	Tok2023d
14490–5807	HDS 2087	28.815	2027.684	0.320	0.1670	111.7	14.4	121.4	3	Tok2023d
16076+0002	HDS 2276	161.761	2024.282	0.774	0.6006	172.0	172.1	71.5	5	Tok2018i
16120–1928	CHR 146 Aa,Ab	10.061	2014.987	0.920	0.0733	346.4	118.9	89.7	3	Tok2021f
16161–3037	I 1586 AB	180.000	2110.616	0.129	0.3347	145.6	133.4	154.6	4	Tok2019c
16385+1240	TOK 727	8.647	2022.391	0.492	0.1009	171.8	316.0	92.9	3	Tok2023d
16536–1045	YSC 156	31.287	2024.604	0.299	0.1076	25.4	129.7	35.6	3	Tok2020g
17184–0147	BAG 51	30.372	2000.506	0.200	0.4637	121.5	309.8	58.2	4	Tok2023d
17535–0355	TOK 54	47.309	2032.612	0.242	0.0928	151.1	0.0	180.0	4	Tok2023d
19301–4904	HDS 2772	290.000	2019.614	0.823	0.5913	175.9	111.2	64.4	4	Tok2017c
19369–6949	GKM Aa,Ab	2.013	2015.363	0.154	0.0239	208.1	42.8	142.3	4	SOAR2023
19561–3208	BWL 53 Ba,Bb	20.000	2025.372	0.522	0.1529	33.6	45.6	55.0	3	Tok2023a

Table 4 *continued*

Table 4 (continued)

WDS	Discoverer	P	T	e	a	Ω	ω	i	Grade	Ref.
α, δ (2000)	Designation	(yr)	(yr)		(arcsec)	(deg)	(deg)	(deg)		
20205–2749	RST 3255	54.643	2027.239	0.929	0.1011	266.9	0.0	0.0	3	Hei1996a
22006–1345	HU 282	500.000	2029.823	0.900	0.4846	102.4	93.1	25.1	4	Tok2023d
22343+0345	HDS 3201	27.770	2000.161	0.451	0.1221	36.8	98.0	52.0	3	Tok2023d
23025–4605	I 1462	155.000	2035.714	0.619	0.1943	105.0	282.4	160.0	4	Tok2023d
23052–1822	B 1898	119.895	1912.955	0.406	0.2569	236.3	94.2	116.8	4	SOAR2023
23210–0229	LSC 107	35.000	2015.328	0.575	0.1327	176.1	13.4	27.4	4	Tok2022f
23224–6516	HDS 3328	45.095	2022.798	0.679	0.1432	110.2	134.9	69.3	3	Tok2022f
23384–2922	B 606	182.729	2035.648	0.000	0.3177	175.7	0.0	83.7	4	SOAR2023

3.4. Combined Spectro-Interferometric Orbits

In calculation of eight orbits we used the radial velocities (RVs), fitting combined spectro-visual orbits. In addition to the visual elements in Table 3, we provide in Table 5 the RV amplitudes of the primary and secondary components K_1 , K_2 and the systemic velocity V_0 . These parameters, delivered by the combined fits of positions and RVs, are similar but not equal to the published spectroscopic elements. The first three columns repeat the WDS codes, DDs, and periods, and the last column gives references to publications containing the RVs used here. In the combined orbits, the angles Ω and ω are selected to match the ascending node and RV of the primary component and the relative positions of the secondary component.

Three combined spectro-interferometric orbits in Figure 3 illustrate different contributions of the RV data to the combined solutions. The double-lined spectroscopic orbit of 01406+0846 (HD 10262, TOK 872, spectral type F2) with a period of 5.85 yr was published by Griffin (2007). The RVs from his paper strongly constrain the orbital period. However, the RV amplitudes of 16.0 and 16.1 km s⁻¹ derived by Griffin, together with the inclination, correspond to the nearly equal component’s masses of 2.24 M_\odot and contradict the substantial magnitude difference of $\Delta y = 1.2$ mag measured at SOAR. The large scatter in the RV curve attests to the uncertain splitting of the blended lines used to derive the RVs. Spectroscopy with a higher resolution and future less biased parallax from Gaia that would explicitly account for the orbital motion will eventually lead to accurate measurement of the masses. All position measures come from SOAR; it was unresolved in 2022 near the periastron, when the secondary moved to the opposite quadrant.

The second example in Figure 3, 12018–3439 (I 215, HD 104471) is a classical long-period visual pair. Spectroscopy revealed this as a triple-lined star containing a 148-day inner subsystem (Tokovinin et al. 2015b). The RVs of both visual components (center of mass of the inner binary and the visual secondary) help somewhat in constraining the eccentricity. Here, the century-long historic visual data, although less accurate than speckle, are essential in providing nearly complete coverage of the orbit. Further improvement of this orbit will be painfully slow. The third example, 14509–1603 (BEU 19 Ba,Bb, HD 130819, α^1 Lib), refers to the spectroscopic subsystem paired to the bright star α^2 Lib (HD 130841) at 231'', which is itself a 70-day spectroscopic binary. The RVs of Ba are taken from the seminal paper by Duquennoy & Mayor (1991). The pair Ba,Bb has been resolved by J.-L. Beuzit in 2004, while all other measures come from SOAR. The magnitude difference is ~ 4.5 mag in the I filter, so the measures are less accurate than usual.

Combined visual-spectroscopic orbits allow measurement of the component’s masses and distances independently of the trigonometric parallax (e.g. Pourbaix 2000). However, the masses are proportional to the cube of the RV amplitudes and to $\sin^3 i$, therefore high accuracy of these parameters is required for getting usefully accurate masses. The example of 01406+0846 above shows that the small RV amplitudes cannot be trusted, and the masses based on the combined orbit are misleading. On the other hand, the double-lined spectroscopic orbit of 12114–1647 with a period of 211 days is quite accurate, but its semimajor axis of 25.3 mas, at the limit of the SOAR resolving power, is too small for measuring accurate masses (the inclination is poorly constrained). The only pair in Table 5 with sufficiently accurate speckle and RV data is 15006+0836 (HIP 73449); the masses are 0.902 ± 0.008 and $0.899 \pm 0.008 M_\odot$ and the orbital parallax is 26.31 ± 0.15 mas. The GDR3 parallax of 26.26 ± 0.16 mas is in agreement because the components are nearly equal and the photocenter is little

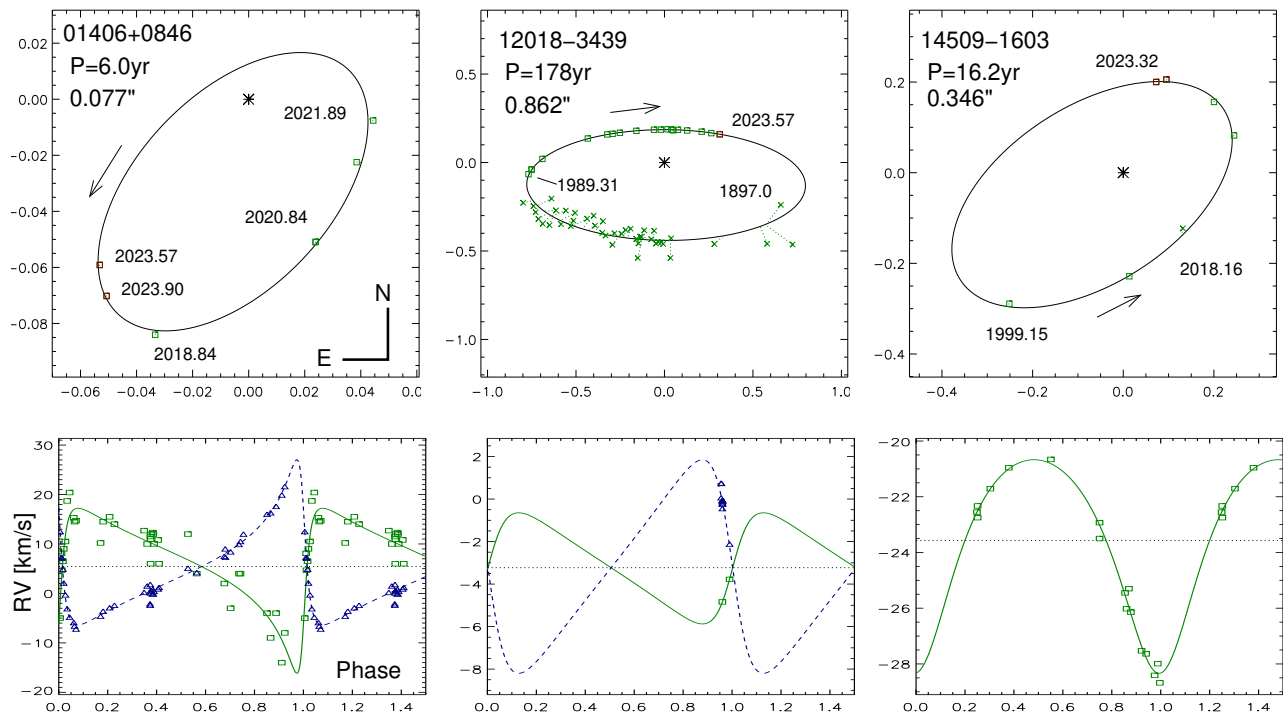


Figure 3. Three combined spectro-interferometric orbits. The upper plots are similar to those in Figure 2, the corresponding RV curves are shown below.

Table 5. Combined Spectro-Interferometric Orbits

WDS	Discoverer	P	K_1	K_2	V_0	Reference
α, δ (2000)	Designation	(yr)	(km s^{-1})	(km s^{-1})	(km s^{-1})	
01406+0846	TOK 872	5.979	16.69	16.70	5.43	Griffin (2007)
		± 0.026	± 1.08	± 0.28	± 0.11	
12018-3439	I 215 AB	178.48	2.61	5.02	-3.23	Tokovinin et al. (2015b)
		± 4.50	± 0.31	± 0.31	± 0.14	
12114-1647	S 634 Aa,Ab	0.5792	15.48	17.71	2.35	Tokovinin (2019)
		± 0.0006	± 0.04	± 0.04	± 0.02	
13133+1621	DOC 1	25.44	6.04	6.53	-7.01	Griffin (2017)
		± 0.17	± 0.13	± 0.13	± 0.09	
13513-2423	WSI 77	10.490	6.18	...	5.27	Willmarth et al. (2016)
		± 0.006	± 0.04	...	± 0.03	
14509-1603	BEU 19 Ba,Bb	16.229	3.83	...	-23.57	Duquennoy & Mayor (1991)
		± 0.043	± 0.12	...	± 0.09	
15006+0836	YSC 8	6.922	10.19	10.23	8.13	Halbwachs et al. (2020)
		± 0.003	± 0.05	± 0.04	± 0.02	
23126+0241	A 2298 AB	29.161	5.24	8.04	34.48	Pourbaix (2000)
		± 0.054	± 0.14	± 0.25	± 0.11	

affected by the orbital motion. This is not the case for the majority of close visual pairs with absent or biased GDR3 parallaxes.

3.5. Hierarchies within 100 pc

During 2021-2022, HRCam has been used to probe components of 1200 wide binaries located within 100 pc

that had indications of unresolved inner subsystems in the Gaia data; about half of those targets were actually resolved, as reported by Tokovinin (2023c). The remaining half are likely beyond the speckle detection limit, either too close and/or with large contrast. In 2023 we revisited some of those new pairs, mostly the closest ones. The goal was twofold. First, to determine

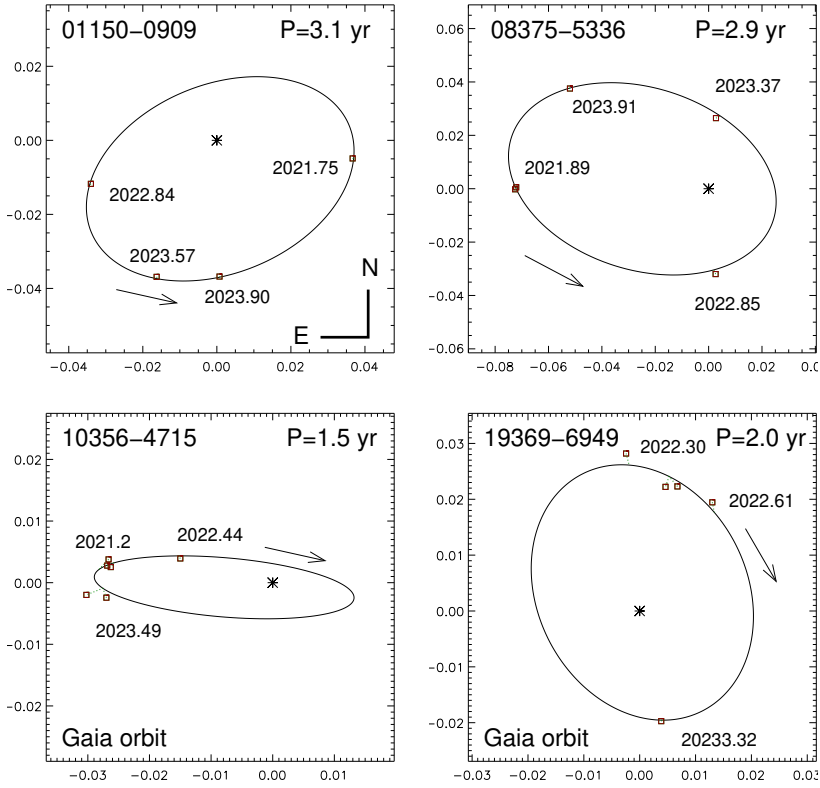


Figure 4. Orbits of four inner pairs in nearby hierarchical systems. The axis scale is in arcseconds.

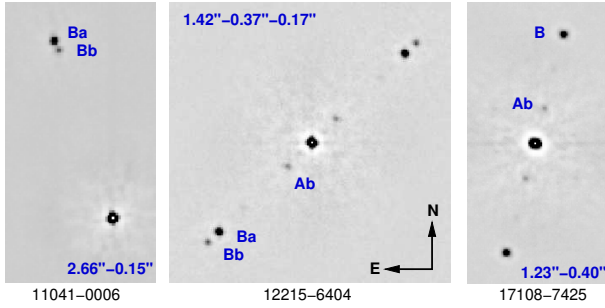


Figure 5. Fragments of speckle auto-correlation functions (ACFs) of three newly identified compact hierarchies within 100 pc (in arbitrary negative rendering). Outer and inner separations are indicated, and the ACF peaks corresponding to true companion locations are labeled.

the sense of motion which, when combined with the Gaia astrometry of the outer components, gives statistical information on the relative orbit orientation. Second, to collect data for determination of inner orbits.

Figure 4 presents the first preliminary orbits of inner subsystems in nearby hierarchies derived from the HRCam data. Two pairs in the top row have four measurements each covering most of their 3-yr orbits. The two remaining pairs have astrometric and spectroscopic orbits in the GDR3, and we fixed some elements to those values while fitting the speckle measurements. Elements

of these orbits are given in the Tables 3 and 4. Continued speckle monitoring of nearby hierarchies from this program will yield more inner orbits in the near future.

The original 100-pc program, started in 2021, targeted pairs wider than $3''$ with reliable Gaia astrometry of both components. It was later extended to pairs with separations from $1''$ to $3''$, and more such pairs were observed during 2023 at low priority. In ten pairs, the expected inner subsystems were actually resolved, and one of them was revealed as a 2+2 quadruple. Representative results are shown in Figure 5. The first triple, 11041–0006, is quite typical: its secondary component was resolved into a $0''.15$ pair Ba,Bb; this system with the outer separation of $2''.66$ is fairly hierarchical. Most newly resolved triples are similarly hierarchical. However, the 2+2 quadruple 12215–6404 (FP Gru, K3.5e) illustrated in the middle panel is not so hierarchical, the ratio of separations in the outer Aa,Ba and inner Aa,Ab pairs is only 3.8, not far from the limit of dynamical stability. Interestingly, this quadruple has a linear configuration, suggesting coplanar orbits if it is viewed edge-on. These stars are chromospherically active and likely young. The triple system 17108–7425 (HIP 84035, G2V) in the right-hand panel is even more extreme in terms of its separation ratio of 3.1, and it is also arranged linearly; the projected separations suggest

periods between 100 and 600 yr. There is also a common proper motion companion at $734''$ (LDS 582 AC) with a projected separation of 53kau that might be either gravitationally bound or simply co-moving.

Weakly hierarchical systems of low-mass stars in the solar neighborhood are amenable to the study of their dynamics, while explaining their origin challenges star formation theory. The prototype of such systems, LHS 1070 (00247–2653), is being monitored at SOAR, and deviations from the Keplerian motion in the inner orbit caused by interaction with the outer star are measurable. The SOAR speckle program has revealed several more weak low-mass hierarchies, to which we add two here.

3.6. Spurious Pairs

Table 6. Likely Spurious Pairs

WDS	Discoverer	Resolved	Unresolved ^a
00374–3717	I 705	0 $''$.4 Vis 1910	2008–23, S, R
00558–1832	B 645	0 $''$.2 Vis 1926	2008–23, R
05484+0745	JNN 267	1 $''$.6 Spe 2011	2023, L
09407–6639	TDS6731	0 $''$.5 Tycho	2023, R
10328+0918	WRH 19	0 $''$.1 Vis 1937	2009–23
10341+1222	CHR 31	0 $''$.2 Spe 1983	2023
11006+0337	CHR 33	0 $''$.2 Spe 1983	2014–23, S, R
11479+0815	CHR 134 Aa,Ab	0 $''$.3 Spe 1987	2014–23, S, R
11518–0546	CHR 36	0 $''$.2 Spe 1983	2014–23, L, R
15355–1447	WRH 20 Aa,Ab	0 $''$.1 Vis 1937	2009–23
16133+1332	CHR 52 Aa,Ab	0 $''$.2 Spe 1983	2008–23, S, R
17376–1524	ISO 6 Aa,Ab	0 $''$.3 Spe 1987	2023
18073+0934	STT 342 Aa,Ab	1 $''$.5 Vis 1842	2023
19247+0833	WSI 108	0 $''$.1 Spe 2008	2015–23, S, R
19255+0307	BNU 6 Aa,Ab	0 $''$.1 Spe 1979	2015–23
20285–2410	CHR 98	0 $''$.2 Spe 1983	2014–23
21400+0911	CHR 105 AB	0 $''$.3 Spe 1982	2008–23
23157+0118	CHR 141 AB	0 $''$.1 Spe 1986	2013–23, S

^a Additional indications of the spurious nature of visual pairs: R – no excess noise in GDR3, RUWE<2; L – long estimated period; S – short estimated period or spectroscopic coverage.

Some double stars listed in the WDS are actually single. These spurious pairs originate from erroneous visual resolutions, dubious speckle data caused by instrumental artifacts, and for other reasons. Identifying spurious pairs will save observing time in the future by eliminating the need to followup and examine these targets. In Table 6 are listed pairs we identify as likely spurious, continuing the clean-up effort from our previous papers. In this table we provide the WDS identifier and DD, the method and date of the original discovery, and the year(s) it has been unresolved in this program. Following that is a code giving other indications supporting the

characterization of the double as spurious (see details in Tokovinin et al. 2022). In the WDS (Mason et al. 2001), these pairs are not removed but are given an **X** code identifying them as a “dubious double” or a “bogus binary”.

4. SUMMARY AND OUTLOOK

Binary stars observed in this program illustrate progress in this field, from historic visual discoveries to Hipparcos and speckle pairs resolved at the end of the 20th century and to the modern, sometimes quite recent, resolutions. The Gaia mission becomes a major driver of speckle programs, in a similar role as played by Hipparcos, but on a much greater scale.

The GDR3 data already include a million new pairs (El-Badry et al. 2021), almost an order of magnitude more than the content of the WDS. However, these wide Gaia pairs move slowly and are not amenable to calculation of orbits in the near future. The historic micrometer pairs, in contrast, have a larger time coverage and, despite the low accuracy of old measures, their monitoring at SOAR steadily produces new orbital solutions. Eventually, the resource of historic pairs will be exhausted, although incremental improvement of their orbits will continue for a long time, until they are fully covered by accurate measures.

An increasing number of new visual orbits is being computed for the tight and fast pairs discovered recently by speckle. The 10^5 Gaia astrometric orbits outnumber the catalog of visual orbits by two orders of magnitude. Future Gaia data releases will further increase the number of astrometric orbits and will extend their maximum periods from 3 to 10 years. However, actual resolution of astrometric binaries by speckle interferometry is needed for measurement of their masses (see Figure 1). Two relevant examples are shown in lower panel of Figure 4. Furthermore, the range of periods from 10 to 100 yr will not be accessible to Gaia without complementary ground-based data, and obtaining this data sooner rather than later will provide the required time coverage. This period range corresponds to the maximum of the period distribution of low-mass stars and matches the periods of massive planets in the solar system. The match is not coincidental because formation of both binaries and planets is related to the typical size of circumstellar disks, 10-100 au.

The Gaia catalog of nearby stars within 100pc contains 61644 stars brighter than $G = 12$ mag; 16315 of those (26%) are likely binaries, based on the increased astrometric noise or double transits. If half of these candidates can be resolved by speckle interferometry, as indicated by the recent survey (Tokovinin 2023c), there

are potentially 8000 targets for future orbits. For comparison, the WDS contains about 12600 pairs closer than $0''.5$, but most of these pairs are too distant and too slow for orbit determination. So, Gaia becomes the major driver of future speckle programs and future work on orbits

Considering the large number of potential speckle targets, one may ask whether it is necessary to observe all of them. A much smaller sample of *accurate* orbits and parallaxes will suffice to address the classical issue of stellar masses and the calibration of stellar evolutionary models. Current projects in this area focus on the less explored mass ranges, i.e. small (Mann et al. 2019; Vrijmoet et al. 2022) or large masses. However, accurate orbits of massive, close, and bright pairs are better determined by long-baseline interferometers than by speckle. But the role of visual orbits is much wider than just mass measurements. The SOAR speckle program concentrates on the dynamics of stellar hierarchical systems (e.g. Tokovinin 2023b). Orbits of exoplanet hosts (Lester et al. 2023) or of very young stars are other interesting research areas. Looking into the future, we foresee an increased demand for speckle astrometry of

binary stars driven by diverse astrophysical applications and stimulated by Gaia.

We thank the SOAR operators for efficient support of this program, and the SOAR director J. Elias for allocating some technical time. R.A.M and E.C acknowledge support from the Vicerrectoria de Investigacion y Desarrollo (VID) de la Universidad de Chile, project number ENL02/23, and from the FONDECYT grant number 1240049. The research of A.T. is supported by the NSF's NOIRLab.

This work used the SIMBAD service operated by Centre des Données Stellaires (Strasbourg, France), bibliographic references from the Astrophysics Data System maintained by SAO/NASA, and the Washington Double Star Catalog maintained at the USNO. This work has made use of data from the European Space Agency (ESA) mission Gaia (<https://www.cosmos.esa.int/gaia>) processed by the Gaia Data Processing and Analysis Consortium (DPAC, <https://www.cosmos.esa.int/web/gaia/dpac/consortium>). Funding for the DPAC has been provided by national institutions, in particular the institutions participating in the Gaia Multilateral Agreement.

Facility: SOAR

REFERENCES

- Abt, H. A., & Levy, S. G. 1985, ApJS, 59, 229, doi: [10.1086/191070](https://doi.org/10.1086/191070)
- Brendley, M., & Mason, B. D. 2007, IAU Commission 26 Information Circular, 163, 1
- Calissendorff, P., Janson, M., Rodet, L., et al. 2022, A&A, 666, A16, doi: [10.1051/0004-6361/202142766](https://doi.org/10.1051/0004-6361/202142766)
- Clark, A., & Dawes, W. R. 1857, MNRAS, 17, 257, doi: [10.1093/mnras/17.9.257](https://doi.org/10.1093/mnras/17.9.257)
- Duquenois, A., & Mayor, M. 1991, A&A, 500, 337
- El-Badry, K., Rix, H.-W., & Heintz, T. M. 2021, MNRAS, 506, 2269, doi: [10.1093/mnras/stab323](https://doi.org/10.1093/mnras/stab323)
- Gaia Collaboration, Brown, A. G. A., Vallenari, A., et al. 2021, A&A, 649, A1, doi: [10.1051/0004-6361/202039657](https://doi.org/10.1051/0004-6361/202039657)
- . 2016, A&A, 595, A2, doi: [10.1051/0004-6361/201629512](https://doi.org/10.1051/0004-6361/201629512)
- Griffin, R. F. 2007, The Observatory, 127, 379
- . 2017, The Observatory, 137, 8
- Halbwachs, J. L., Kiefer, F., Lebreton, Y., et al. 2020, MNRAS, 496, 1355, doi: [10.1093/mnras/staa1571](https://doi.org/10.1093/mnras/staa1571)
- Hall, A. 1892, Observations made at the U.S. Naval Observatory, 6, E.1
- Hartkopf, W. I., Mason, B. D., & Worley, C. E. 2001, AJ, 122, 3472, doi: [10.1086/323921](https://doi.org/10.1086/323921)
- Hartkopf, W. I., Tokovinin, A., & Mason, B. D. 2012, AJ, 143, 42, doi: [10.1088/0004-6256/143/2/42](https://doi.org/10.1088/0004-6256/143/2/42)
- Henry, G. W., Fekel, F. C., & Henry, S. M. 2011, AJ, 142, 39, doi: [10.1088/0004-6256/142/2/39](https://doi.org/10.1088/0004-6256/142/2/39)
- Horch, E. P., van Belle, G. T., Davidson, James W., J., et al. 2015, AJ, 150, 151, doi: [10.1088/0004-6256/150/5/151](https://doi.org/10.1088/0004-6256/150/5/151)
- Horch, E. P., Casetti-Dinescu, D. I., Camarata, M. A., et al. 2017, AJ, 153, 212, doi: [10.3847/1538-3881/aa6749](https://doi.org/10.3847/1538-3881/aa6749)
- Horch, E. P., Tokovinin, A., Weiss, S. A., et al. 2019, AJ, 157, 56, doi: [10.3847/1538-3881/aaf87e](https://doi.org/10.3847/1538-3881/aaf87e)
- Kostov, V. B., Powell, B. P., Rappaport, S. A., et al. 2022, ApJS, 259, 66, doi: [10.3847/1538-4365/ac5458](https://doi.org/10.3847/1538-4365/ac5458)
- Lagrange, A. M., Desort, M., Galland, F., Udry, S., & Mayor, M. 2009, A&A, 495, 335, doi: [10.1051/0004-6361:200810105](https://doi.org/10.1051/0004-6361:200810105)
- Lester, K. V., Howell, S. B., Matson, R. A., et al. 2023, AJ, 166, 166, doi: [10.3847/1538-3881/acf563](https://doi.org/10.3847/1538-3881/acf563)
- Mann, A. W., Dupuy, T., Kraus, A. L., et al. 2019, ApJ, 871, 63, doi: [10.3847/1538-4357/aaf3bc](https://doi.org/10.3847/1538-4357/aaf3bc)
- Marion, L., Absil, O., Ertel, S., et al. 2014, A&A, 570, A127, doi: [10.1051/0004-6361/201424780](https://doi.org/10.1051/0004-6361/201424780)

- Mason, B. D., Tokovinin, A., Mendez, R. A., & Costa, E. 2023, *AJ*, 166, 139, doi: [10.3847/1538-3881/acedaf](https://doi.org/10.3847/1538-3881/acedaf)
- Mason, B. D., Wycoff, G. L., Hartkopf, W. I., Douglass, G. G., & Worley, C. E. 2001, *AJ*, 122, 3466, doi: [10.1086/323920](https://doi.org/10.1086/323920)
- Mendez, R. A., Claveria, R. M., Orchard, M. E., & Silva, J. F. 2017, *AJ*, 154, 187, doi: [10.3847/1538-3881/aa8d6f](https://doi.org/10.3847/1538-3881/aa8d6f)
- Pourbaix, D. 2000, *A&AS*, 145, 215, doi: [10.1051/aas:2000237](https://doi.org/10.1051/aas:2000237)
- Powell, B. P., Kostov, V. B., & Tokovinin, A. 2023, *MNRAS*, 524, 4296, doi: [10.1093/mnras/stad2065](https://doi.org/10.1093/mnras/stad2065)
- Tokovinin, A. 2012, *AJ*, 144, 56, doi: [10.1088/0004-6256/144/2/56](https://doi.org/10.1088/0004-6256/144/2/56)
- . 2016, ORBIT: IDL software for visual, spectroscopic, and combined orbits, Zenodo, doi: [10.5281/zenodo.61119](https://doi.org/10.5281/zenodo.61119)
- . 2018a, *ApJS*, 235, 6, doi: [10.3847/1538-4365/aaa1a5](https://doi.org/10.3847/1538-4365/aaa1a5)
- . 2018b, *PASP*, 130, 035002, doi: [10.1088/1538-3873/aaa7d9](https://doi.org/10.1088/1538-3873/aaa7d9)
- . 2019, *AJ*, 158, 222, doi: [10.3847/1538-3881/ab4c94](https://doi.org/10.3847/1538-3881/ab4c94)
- . 2021a, *Universe*, 7, 352, doi: [10.3390/universe7090352](https://doi.org/10.3390/universe7090352)
- . 2021b, *AJ*, 161, 144, doi: [10.3847/1538-3881/abda42](https://doi.org/10.3847/1538-3881/abda42)
- . 2022, *AJ*, 163, 127, doi: [10.3847/1538-3881/ac4bc5](https://doi.org/10.3847/1538-3881/ac4bc5)
- . 2023a, *AJ*, 165, 160, doi: [10.3847/1538-3881/acbe42](https://doi.org/10.3847/1538-3881/acbe42)
- . 2023b, *AJ*, 165, 165, doi: [10.3847/1538-3881/acbf32](https://doi.org/10.3847/1538-3881/acbf32)
- . 2023c, *AJ*, 165, 180, doi: [10.3847/1538-3881/acc464](https://doi.org/10.3847/1538-3881/acc464)
- Tokovinin, A., Cantarutti, R., Tighe, R., et al. 2010a, *PASP*, 122, 1483, doi: [10.1086/657903](https://doi.org/10.1086/657903)
- Tokovinin, A., & Latham, D. W. 2020, *AJ*, 160, 251, doi: [10.3847/1538-3881/abbad4](https://doi.org/10.3847/1538-3881/abbad4)
- Tokovinin, A., Mason, B. D., & Hartkopf, W. I. 2010b, *AJ*, 139, 743, doi: [10.1088/0004-6256/139/2/743](https://doi.org/10.1088/0004-6256/139/2/743)
- . 2014, *AJ*, 147, 123, doi: [10.1088/0004-6256/147/5/123](https://doi.org/10.1088/0004-6256/147/5/123)
- Tokovinin, A., Mason, B. D., Hartkopf, W. I., Mendez, R. A., & Horch, E. P. 2015a, *AJ*, 150, 50, doi: [10.1088/0004-6256/150/2/50](https://doi.org/10.1088/0004-6256/150/2/50)
- . 2016, *AJ*, 151, 153, doi: [10.3847/0004-6256/151/6/153](https://doi.org/10.3847/0004-6256/151/6/153)
- . 2018, *AJ*, 155, 235, doi: [10.3847/1538-3881/aabf8d](https://doi.org/10.3847/1538-3881/aabf8d)
- Tokovinin, A., Mason, B. D., Mendez, R. A., & Costa, E. 2022, *AJ*, 164, 58, doi: [10.3847/1538-3881/ac78e7](https://doi.org/10.3847/1538-3881/ac78e7)
- Tokovinin, A., Mason, B. D., Mendez, R. A., Costa, E., & Horch, E. P. 2020, *AJ*, 160, 7, doi: [10.3847/1538-3881/ab91c1](https://doi.org/10.3847/1538-3881/ab91c1)
- Tokovinin, A., Mason, B. D., Mendez, R. A., et al. 2021, *AJ*, 162, 41, doi: [10.3847/1538-3881/ac00bd](https://doi.org/10.3847/1538-3881/ac00bd)
- Tokovinin, A., Mason, B. D., Mendez, R. A., Horch, E. P., & Briceño, C. 2019, *AJ*, 158, 48, doi: [10.3847/1538-3881/ab24e4](https://doi.org/10.3847/1538-3881/ab24e4)
- Tokovinin, A., Pribulla, T., & Fischer, D. 2015b, *AJ*, 149, 8, doi: [10.1088/0004-6256/149/1/8](https://doi.org/10.1088/0004-6256/149/1/8)
- Vrijmoet, E. H., Tokovinin, A., Henry, T. J., et al. 2022, *AJ*, 163, 178, doi: [10.3847/1538-3881/ac52f6](https://doi.org/10.3847/1538-3881/ac52f6)
- Willmarth, D. W., Fekel, F. C., Abt, H. A., & Pourbaix, D. 2016, *AJ*, 152, 46, doi: [10.3847/0004-6256/152/2/46](https://doi.org/10.3847/0004-6256/152/2/46)
- Ziegler, C., Tokovinin, A., Briceño, C., et al. 2020, *AJ*, 159, 19, doi: [10.3847/1538-3881/ab55e9](https://doi.org/10.3847/1538-3881/ab55e9)
- Ziegler, C., Tokovinin, A., Latiolais, M., et al. 2021, *AJ*, 162, 192, doi: [10.3847/1538-3881/ac17f6](https://doi.org/10.3847/1538-3881/ac17f6)